Velocity circulation intermittency in finite-temperature turbulent superfluid helium

Nicolás P. Müller,[1] Yuan Tang,[2,3] Wei Guo,[2,3] and Giorgio Krstulovic[1]
[1]*Université Côte d'Azur, Observatoire de la Côte d'Azur, CNRS, Laboratoire Lagrange, Boulevard de l'Observatoire CS 34229 - F 06304 NICE Cedex 4, France*
[2]*National High Magnetic Field Laboratory, 1800 East Paul Dirac Drive, Tallahassee, Florida 32310, USA*
[3]*Mechanical Engineering Department, FAMU-FSU College of Engineering, Florida State University, Tallahassee, Florida 32310, USA*

(Received 27 April 2022; accepted 22 September 2022; published 11 October 2022)

We study intermittency of circulation moments in turbulent superfluid helium by using experimental grid turbulence and numerical simulations of the Hall-Vinen-Bekarevich-Khalatnikov model. More precisely, we compute the velocity circulation Γ_r in loops of size r laying in the inertial range. For both experimental and numerical data, the circulation variance shows a clear Kolmogorov scaling $\langle \Gamma_r^2 \rangle \sim r^{8/3}$ in the inertial range, independently of the temperature. Scaling exponents of high-order moments are comparable, within error bars, to previously reported anomalous circulation exponents in classical turbulence and low-temperature quantum turbulence numerical simulations.

DOI: 10.1103/PhysRevFluids.7.104604

I. INTRODUCTION

Turbulence, the disordered and chaotic motion of fluids, is an ubiquitous phenomenon in nature taking place at very different length scales, from astrophysical to microscales [1]. Its dynamics is described by complex velocity fields dominated by vortices, regions of the flow with a strong local rotation. Despite great efforts and improvements made on its understanding over the last two centuries, there is still no full theory able to describe the dynamics of turbulent flows completely.

The most traditional way of characterizing velocity fluctuations in classical turbulence (CT) at a given scale $r = |\boldsymbol{r}|$ is using the so-called structure functions $S_p(r) = \langle [\boldsymbol{v}(\boldsymbol{x}+\boldsymbol{r}) - \boldsymbol{v}(\boldsymbol{x})]^p \rangle$, where the brackets indicate an average in space, time, or over different ensembles. When a large scale separation exists between the forcing scale L and the dissipative scale η, the structure function displays power laws as $S_p(r) \sim r^{\zeta_p}$ for $\eta \ll r \ll L$. For homogeneous isotropic flows, in 1941 Kolmogorov predicted the self-similar scaling $\zeta_p^{\mathrm{K41}} = p/3$ (K41 prediction) [2]. Such a prediction is based on a mean-field approach and simply based on dimensional analysis. Experiments and numerical simulations on homogeneous isotropic CT have, however, showed some deviations from K41 theory [3]. This breakdown of self-similarity is usually attributed to the highly intermittent nature of velocity fluctuations at small scales. There are several phenomenological theories based on multifractality intending to describe the intermittency of turbulent flows [4–6].

A different system with a manifest intermittency is quantum turbulence (QT), the turbulence taking place in superfluids [7]. When liquid ^{4}He is cooled below the critical temperature of $T_\lambda = 2.17$ K, it undergoes a phase transition into a superfluid state [8]. Its dynamics at nonzero temperatures can be interpreted as two-fluid systems that mutually interact between themselves: a superfluid component with a velocity field $\boldsymbol{v}_\mathrm{s}$ that presents no viscosity, and a normal viscous component $\boldsymbol{v}_\mathrm{n}$ that is described by the classical Navier–Stokes equations [9]. These two components

can move in phase (coflow) or in counterphase (counterflow). In the first case, it has been observed both in experiments and numerical simulations that the statistical properties of the flow at large scales follows a behavior similar to classical fluids [10]. On the other hand, counterflow turbulence dynamics differs from classical fluids, displaying an inverse energy cascade and a breakdown of isotropy at small scales [11,12].

In superfluid ^{4}He, the relative densities between the normal and superfluid components depend on temperature, and therefore there is an open discussion on whether or not there is a dependence of intermittency on the temperature. Experimental studies on QT at the wake of a disk in superfluid ^{4}He at temperatures between 1.3 K $\leqslant T \leqslant T_\lambda$ show that there is no temperature dependence on the intermittency [13]. Other sets of experiments on homogeneous isotropic QT show that there is no temperature dependence up to $p = 6$, but there are some deviations from CT [14,15]. Numerical simulations on QT using different models like the Gross-Pitaevskii (GP) equation, shell models, or the HVBK (Hall-Vinen-Bekarevich-Khalatnikov) equations show a clear temperature dependence that is amplified at intermediate temperatures of $1.8 \leqslant T \leqslant 2$ K, where the density fractions of each component approach each other [16,17]. However, some HVBK-based shell models show an enhancement of intermittency on this temperature range while others show some decrease or even nonintermittent behavior [18,19]. Given the lack of consensus between experiments and numerical simulations, further studies are required on this subject.

An alternative way of studying intermittency in turbulent flows is using moments of the velocity circulation instead of the velocity increments [20–23]. The velocity circulation around a closed loop $\mathcal{C}$ enclosing an area A is defined by

$$\Gamma_A(\mathcal{C}; \boldsymbol{v}) = \oint_{\mathcal{C}} \boldsymbol{v} \cdot d\boldsymbol{l} = \iint_A \boldsymbol{\omega} \cdot \boldsymbol{n}\, dS, \tag{1}$$

where in the second equality we make use of the Stokes theorem, with $\boldsymbol{\omega} = \boldsymbol{\nabla} \times \boldsymbol{v}$ the vorticity field. First theoretical studies on the statistics of velocity circulation suggested that the probability density function (PDF) follows the area rule, that is, within the inertial range of scales, they depend only on the minimal area circumscribed by the closed loop [20,24]. Further numerical studies at low Reynolds numbers suggested that velocity circulation is a highly intermittent quantity, as well as velocity increments [21–23]. These results were also observed in experiments of homogeneous and isotropic turbulence in classical fluids [25]. It was recently shown using high-resolution numerical simulations of the Navier–Stokes equations that the moments of circulation present a clear scaling,

$$\left\langle \Gamma_r^p \right\rangle \sim r^{\lambda_p}, \text{ for } \quad \eta \ll r \ll L, \tag{2}$$

with $r = \sqrt{A}$, which deviate from Kolmogorov-based prediction $\lambda_p^{\mathrm{K41}} = 4p/3$ for larger moments [26]. Moreover, in numerical simulations of the GP equation, a model for low-temperature superfluids, a very similar behavior between CT and QT was observed [27]. The advantage of using the velocity circulation to study intermittency is that it is an integral quantity, and allows for the development of new theories for intermittency [28–30]. To our knowledge, there is still no experimental studies in superfluid ^{4}He of the scaling laws of velocity circulation.

In this paper, we study intermittency of superfluid ^{4}He from the point of view of velocity circulation. We measure the circulation scaling in experiments of grid turbulence in superfluid ^{4}He and compare them with numerical simulations of the coarse-grained HVBK equations at different temperatures (see Sec. II for details on the experimental and numerical methods). The analysis is performed for large-scale statistics of QT. We show that for both experiments and numerical simulations, the scaling exponents of low-order moments do not depend significatively on the temperature of the superfluid. In particular, for numerical simulations we show that high-order moments display the same intermittent behavior as in CT. These results are in agreement with the experimental observations of the velocity increments [13,31]. This paper is organized as follows. In Sec. II, we provide details of our experimental and numerical methods, including the model we use and the algorithm for computing the velocity circulation. Then, in Sec. III we present our

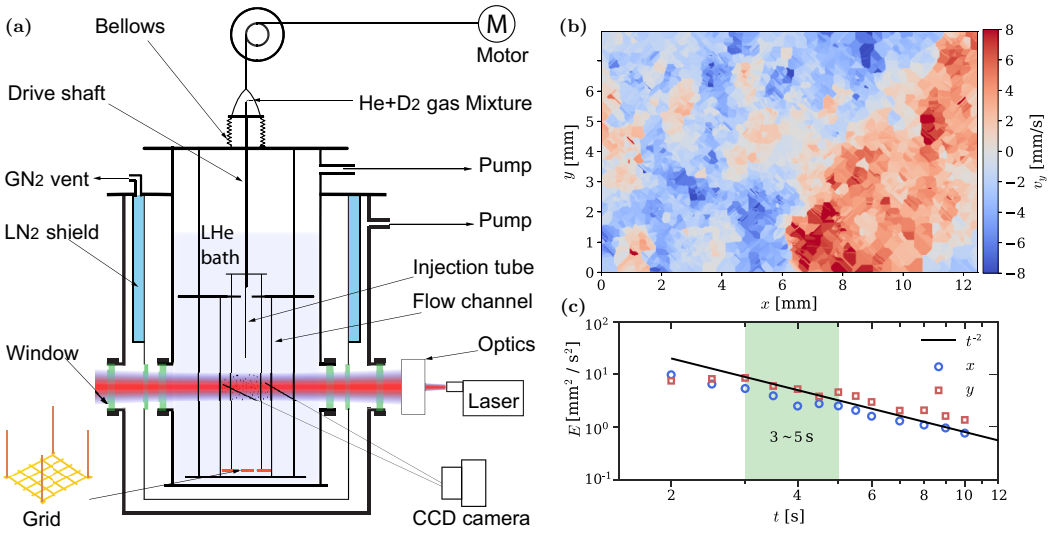

FIG. 1. (a) Experimental apparatus for grid turbulence of the superfluid ^{4}He. (b) Typical experimental velocity field obtained from the PTV measurements of grid turbulence in superfluid ^{4}He following the procedure described in Sec. II A. (c) Turbulent kinetic energy density as a function of decay time for a typical acquisition at $T = 1.95$ K.

experimental and numerical results. Finally, in Sec. IV we summarize our results and discuss known results on the circulation intermittency.

II. EXPERIMENTAL SETUP AND MATHEMATICAL MODEL

A. Experimental setup

To examine the circulation statistics experimentally, we have conducted velocity-field measurements in quasiclassical turbulence generated in He II by a towed grid using the particle tracking velocimetry (PTV) method [15]. The experimental apparatus, shown in Fig. 1(a), consists of a transparent cast acrylic flow channel with a cross-section area of 1.6×1.6 cm^2 and a length of 33 cm immersed vertically in a He II bath (more details of the setup can be found in Ref. [32]). The bath temperature is controlled by regulating the vapor pressure. A brass mesh grid with a spacing of 3 mm and 40% solidity is suspended in the flow channel by stainless-steel thin wires at the four corners. A linear motor outside the cryostat can pull the wires and hence the grid at a speed up to 60 cm/s. In the current paper, we used a fixed grid speed at 30 cm/s. To probe the flow, we adopt the PTV method using solidified D_2 tracer particles with a mean diameter of about 5 μm [32]. These particles are entrained by the viscous normal-fluid flow due to their small sizes and hence small Stokes number [15,33,34], but they can also get trapped on quantized vortices in the superfluid [35–38]. A continuous-wave laser sheet (thickness: 200 μm, height: 9 mm) passes through the center of two opposite side walls of the channel to illuminate the particles. The motion of the particles is then capture by a CCD camera at 200 frames per second at an angle perpendicular to both the flow channel and the laser sheet. The pixel size of the camera is 7.5 μm $\times$ 7.5 μm with a full view resolution of 2560 $\times$ 1440 pixels. We install a Nikon Micro-Nikkor 105 mm f/2.8 lens to the camera so the view region is coupled to the camera sensor at a ratio of nearly 1:1. The exact length scale in the images can be calibrated by measuring the pixel distance between the two side walls of the channel. We set $t = 0$ when the grid passes the center of the view window and typically record the particle motion continuously for 40 s. A modified feature-point tracking routine [32] is adopted to extract the trajectories of the tracer particles from the sequence of images. In the

current paper, we focus on analyzing the data obtained in the time interval $t = 3$ s to $t = 5$ s at two bath temperatures, i.e., $T = 1.65$ K and 1.95 K. The turbulence at these decay times appears to be reasonably homogeneous and isotropic, and its turbulence intensity is relatively high such that an inertial range exists [15].

For circulation analysis, it is more convenient to have two-dimensional Eulerian velocity field. To generate this information using the spatially sparse PTV data, we adopt the method reported in Ref. [39]. We first combine the velocity data $\boldsymbol{v}(x, y)$ obtained from 11 successive images into a single velocity-field image. This procedure assumes that during the acquisition time of these 11 images (i.e., 50 ms), the velocity field does not change considerably, so these data describe a single instantaneous velocity field. Then we divide the combined image into square cells with side length $\Delta = 0.02$ mm so most of the cells have at least 1–2 data points. The velocity assigned to the center of each cell is calculated as the Gaussian-averaged velocity of particles inside the cell with a Gaussian-profile variance $\sigma \approx \Delta/2$ to ensure that the Gaussian weight drops to near zero at the cell's edge. Occasionally, there may not be any particles that fall inside a particular cell. In this case, we increase the size of this cell by a factor of 2, and this process may be repeated until a few particles fall in the enlarged cell so the velocity at the cell center can be determined. A representative resulted velocity field $\boldsymbol{v}(x, y)$ obtained at $T = 1.95$ K is shown in Fig. 1(b) . In Fig. 1(c), we show the time evolution of the turbulent kinetic energy density, defined as $E_{x,y} = \langle \boldsymbol{v}_{x,y}^2 \rangle/2$. At $t \geqslant 3$ s, the kinetic energy density of the velocity components in both x and y directions are comparable, suggesting that the flow is relatively isotropic. Furthermore, a decay scaling $E_{x,y} \propto t^{-2}$ at $t \geqslant 3$ s is clearly visible. This scaling is a characteristic feature of the homogeneous and isotropic turbulence in He II when the size of the energy containing eddies are saturated by the channel width [40]. Here we specifically analyze the data at 3 s $\leqslant t \leqslant 5$ s, since the flow is reasonably homogeneous and isotropic and the turbulent kinetic energy density is relatively large such that a clear inertial range may exist.

To aid the discussion of the statistical analysis, we have also calculated the Taylor microscale $\lambda_{\mathrm{T}} = \sqrt{15\nu/\epsilon}\, v_{\mathrm{rms}}$ and the Taylor Reynolds number $\mathrm{Re}_\lambda = v_{\mathrm{rms}}\lambda_{\mathrm{T}}/\nu$. These calculations involve the evaluation of the energy dissipation rate ϵ. As explained in more detail in our previous work [15], we calculate the energy dissipation rate based on the measured velocity derivatives in the x-y plane. The obtained Re_λ is 40–60, and the corresponding Taylor microscale is 0.15–0.17 mm for 3 s $\leqslant t \leqslant 5$ s at both 1.65 K and 1.95 K.

B. Model for superfluid helium

The dynamics of superfluid helium at finite temperatures and scales larger than the intervortex distance can be described by the coarse-grained HVBK equations [9,18,34,41]:

$$\frac{\partial \boldsymbol{v}_{\mathrm{n}}}{\partial t} + \boldsymbol{v}_{\mathrm{n}} \cdot \boldsymbol{\nabla} \boldsymbol{v}_{\mathrm{n}} = -\frac{1}{\rho_{\mathrm{n}}} \boldsymbol{\nabla} p_{\mathrm{n}} + \nu_{\mathrm{n}} \nabla^2 \boldsymbol{v}_{\mathrm{n}} - \frac{\rho_s}{\rho_n} \boldsymbol{f}_{\mathrm{ns}} + \boldsymbol{\Phi}_{\mathrm{n}}, \tag{3}$$

$$\frac{\partial \boldsymbol{v}_{\mathrm{s}}}{\partial t} + \boldsymbol{v}_{\mathrm{s}} \cdot \boldsymbol{\nabla} \boldsymbol{v}_{\mathrm{s}} = -\frac{1}{\rho_{\mathrm{s}}} \boldsymbol{\nabla} p_{\mathrm{s}} + \nu_{\mathrm{s}} \nabla^2 \boldsymbol{v}_{\mathrm{s}} + \boldsymbol{f}_{\mathrm{ns}} + \boldsymbol{\Phi}_{\mathrm{s}}, \tag{4}$$

$$\boldsymbol{\nabla} \cdot \boldsymbol{v}_{\mathrm{n}} = \boldsymbol{\nabla} \cdot \boldsymbol{v}_{\mathrm{s}} = 0. \tag{5}$$

This incompressible two-fluid model describes the motion of the normal ($\boldsymbol{v}_{\mathrm{n}}$) and superfluid ($\boldsymbol{v}_{\mathrm{s}}$) components via two coupled Navier–Stokes equations. The kinematic viscosity is related to the dynamic one via $\nu_{\mathrm{n}} = \mu/\rho_{\mathrm{n}}$, $p_{\mathrm{n,s}}$ is the hydrodynamic pressure of each component, and the total density of the fluid is $\rho = \rho_{\mathrm{n}} + \rho_{\mathrm{s}}$. The superfluid component also dissipates via an effective viscosity ν_{s} that takes into account dissipative effects taking place at small scales that the HVBK model is not able to resolve, like quantum vortex reconnections and Kelvin waves [42–46]. Both Navier–Stokes equations are coupled through the mutual friction force between both velocity components $\boldsymbol{f}_{\mathrm{ns}} = \alpha \Omega_0 (\boldsymbol{v}_{\mathrm{n}} - \boldsymbol{v}_{\mathrm{s}})$, with $\alpha = \alpha(T)$ the mutual friction coefficient that depends on the temperature of the system. The frequency $\Omega_0 = \kappa \mathcal{L}$ is proportional to the vortex line density $\mathcal{L}$ and to the quantum of circulation of the vortices κ, and can be estimated using the enstrophy Ω as

TABLE I. Table of parameters for the numerical simulations of the HVBK equations. N corresponds to the linear resolution on each direction, T is the temperature of the HVBK system expressed in Kelvin units, α the mutual friction coefficient, ρ_s and ρ_n the superfluid and normal densities, respectively, ν_s/ν_n the ratio of the kinematic viscosities, and $\mathrm{Re}_\lambda^{n,s}$ to the Taylor-microscale Reynolds number $\mathrm{Re}_\lambda = v_{\mathrm{rms}}\lambda_T/\nu$ of the normal and superfluid components, respectively. The Reynolds number $\mathrm{Re}_\lambda^{\mathrm{tot}}$ is associated to the total velocity $\boldsymbol{v}_{\mathrm{tot}} = (\rho_s \boldsymbol{v}_s + \rho_n \boldsymbol{v}_n)/\rho$. The integral length scale is defined as $L_I^{\mathrm{tot}} = \int k^{-1}E(k)dk / \int E(k)dk$.

RUN	N	T (K)	α	ρ_s/ρ	ρ_n/ρ	ν_s/ν_n	Re_λ^n	Re_λ^s	$\mathrm{Re}_\lambda^{\mathrm{tot}}$	L_I^{tot}
I	1024	1.3	0.034	0.952	0.048	0.043	34	412	418	0.56
II	1024	1.5	0.072	0.889	0.111	0.2	187	651	628	0.57
III	1024	1.79	0.156	0.696	0.304	0.8	358	427	389	0.57
IV	1024	1.9	0.206	0.574	0.426	1.25	500	419	462	0.53
V	1024	1.96	0.244	0.504	0.496	1.50	550	410	545	0.57
VI	1024	2.05	0.347	0.362	0.638	1.87	550	345	495	0.54
VII	1024	2.1	0.481	0.259	0.741	2.5	406	193	344	0.56

$\Omega_0^2 \approx \Omega = \langle|\boldsymbol{\omega}_s|^2\rangle/2$ with $\boldsymbol{\omega}_s = \boldsymbol{\nabla}\times\boldsymbol{v}_s$ the superfluid vorticity and $\langle.\rangle$ denoting a spatial average [17,34]. Thus, it is possible to find an estimation of the mean intervortex distance of the flow as $\ell = \mathcal{L}^{-1/2}$. It is important to remark that this relation is not obtained from first principles. An alternative approach is to assume that the intervortex distance is of the order of the Taylor microscale of the turbulent flow $\ell \sim \lambda_T = \sqrt{5E/\Omega}$, with $E = \langle|\boldsymbol{v}|^2\rangle/2$ the mean kinetic energy and $\Omega = \Omega_0^2$ the enstrophy of the flow [47]. We use two independent large-scale constant-in-time Gaussian random forces $\boldsymbol{\Phi}_n(\boldsymbol{x})$ and $\boldsymbol{\Phi}_s(\boldsymbol{x})$ to excite both fluid components and obtain a stationary state.

We study the scaling of velocity circulation in superfluid ^{4}He at different temperatures by solving numerically the HVBK Eqs. (3)–(5) using a fully dealiased Fourier pseudospectral code in a periodic cubic domain and a third-order Runge-Kutta integration in time (see Ref. [48] for details). We perform seven numerical simulations of these equations for temperatures that vary between $T = 1.3$ K and $T = 2.1$ K, using $N = 1024$ linear collocation points in each direction. All the parameters used for each numerical simulation are shown in Table I. The mutual friction, normal, and superfluid density fractions and viscosity ratios were chosen to reproduce the typical values observed experimentally in superfluid helium at each temperature [49,50]. We report the Reynolds number associated to the Taylor-microscale $\mathrm{Re}_\lambda^{n,s,\mathrm{tot}} = v_{\mathrm{rms}}^{n,s,\mathrm{tot}}\lambda_T/\nu_{n,s,\mathrm{tot}}$, where the superscripts correspond to the normal, superfluid and total components, respectively. The total velocity is defined as $\boldsymbol{v}_{\mathrm{tot}} = (\rho_n\boldsymbol{v}_n + \rho_s\boldsymbol{v}_s)/\rho$.

For comparison, we also use data from Refs. [27,28]. In particular, we use the circulation exponents of CT obtained by integrating the Navier-Stokes equations with a Taylor-microscale Reynolds number of $\mathrm{Re}_\lambda = 510$, and zero-temperature QT generated by using the GP model, with a separation between the integral length scale L_I and the healing length ξ of $L_I/\xi = 820$. Using the intervortex distance ℓ as the equivalent of the Taylor microscale in the GP model, we can obtain a microscale Reynolds number of $\mathrm{Re}_\lambda^{\mathrm{GP}} \equiv 15L_I/\ell = 440$. In both cases, the numerical simulations have a linear spatial resolution of $N = 2048$.

C. Data analysis

The velocity circulation for the HVBK numerical simulations is computed using the Fourier coefficients of the velocity fields of each component using our openly available code [51]. Over each two-dimensional L-periodic slab of the system, in three different orientations, we compute the circulation over square loops of different sizes r centered at each point $\boldsymbol{x} = (x, y)$ of the domain as

the convolution [28]

$$\Gamma_r(\boldsymbol{x}) = \int_{S_r(\boldsymbol{x})} \omega_{\mathrm{n,s}}(\boldsymbol{x}')d^2\boldsymbol{x}' = \iint H_r(\boldsymbol{x}-\boldsymbol{x}')\omega_{\mathrm{n,s}}(\boldsymbol{x}')d^2\boldsymbol{x}, \tag{6}$$

where $\omega_{\mathrm{n,s}} = (\boldsymbol{\nabla}_{2\mathrm{D}} \times \boldsymbol{v}_{\mathrm{n,s}}) \cdot \hat{z}$ is the two-dimensional vorticity of the normal or superfluid component for each slab and $S_r(\boldsymbol{x})$ a squared planar surface of linear size r centered at $\boldsymbol{x}$. The convolution kernel is defined as $H_r(\boldsymbol{x}) = \Pi(x/r)\Pi(y/r)$, where $\Pi(x) = 1$ for $|x| < 1/2$ and 0 otherwise, so it can be written in Fourier space in terms of the normalized sinc function as $\hat{H}_r(k_x, k_y) = (r/L)^2 \mathrm{sinc}(k_x r/2\pi)\mathrm{sinc}(k_y r/2\pi)$.

This method can be used to compute the simulations for the normal and superfluid components obtained from the numerical simulations of the HVBK equations due to their periodicity. However, the velocity fields obtained from experiments are not periodic. Therefore, instead of using the Fourier coefficients, we compute the circulation directly from the velocity field following the first equality in Eq. (1). We have checked that the analysis done using this nonperiodic method leads to the same quantitative results for the circulation moments and their scaling exponents obtained using the Fourier coefficients and periodic boundary conditions. In particular, we tested these methods using the velocity fields from the numerical simulations of the HVBK equations.

III. RESULTS

A. Low order statistics from experimental data

We analyze the data obtained from several realizations of grid turbulence in superfluid helium at temperatures $T = 1.65$ K and $T = 1.95$ K following the experimental setup described in Sec. II A. We determine that the system reaches a regime of fully developed turbulence between three and five seconds after the grid passes through the center of the region. We study and obtain a two-dimensional Eulerian velocity field every 0.1 s within this time interval on a rectangular window of 7.98×12.48 mm, following the procedure described in Sec. II A. These velocity fields allow us to compute the velocity circulation around squared planar loops of different linear sizes r, as described in Sec. II C. As the velocity field is not periodic, we analyze a reduced window of $(L_x - r, L_y - r)$, obtaining a reduced amount of statistics for larger loops. In Fig. 1(c), we show that the energy injected may vary between different realizations of the flow, and that within the time interval studied it shows a consistent decaying. Averaging the different realizations and the circulation obtained at different times would give a stronger weight to some realizations and to early times of the evolution. Therefore, we normalize each realization and each time step by the circulation at large scales $\Gamma_0 = v_{\mathrm{rms}} L_{\mathrm{I}}$, with the root mean square velocity field $v_{\mathrm{rms}} = \sqrt{(2v_x^2 + v_y^2)/3}$ of each time step and the mean integral length scale $L_{\mathrm{I}} = \int k^{-1}E(k)dk / \int E(k)dk$, with $E(k)$ the energy spectrum. The typical integral length scale in our experiments is $L_{\mathrm{I}} = 4.5$ mm and the typical root-mean-square velocity is $v_{\mathrm{rms}} = 1.7$ mm/s. Figure 2 shows the variance of the normalized circulation $\tilde{\Gamma} = \Gamma/\Gamma_0$ obtained from the averaged measurements as a function of the linear size of the loop normalized by the Taylor-microscale $\lambda_{\mathrm{T}} \approx 0.16$ mm. In the inertial range, represented by the green-shaded region, the circulation variance follows a scaling that approximates the Kolmogorov one $\lambda_2^{\mathrm{K41}} = 8/3$ for both temperatures. Moreover, when the variances are compensated by λ_2^{K41}, they approach to a plateau. Note that scales in this range are larger than the laser sheet thickness and should be little affected by the construction of the Eulerian field using experimental data.

Figure 3 shows the PDFs of the velocity circulation for both temperatures and for different loop sizes (in green). At small scales, the PDFs present heavy tails, a clear signature of intermittency. As the size of the loop increases, they collapse and approach a Gaussian distribution (red dashed line). This behavior is similar to the one observed for the velocity circulation in numerical simulations of the Navier–Stokes and GP equations [26–28], and experiments in classical fluids [25].

The study of high-order moments of the circulation $\langle \Gamma^p \rangle$ usually requires a large amount of data for statistical convergence [52]. Measured moments of order p cannot be trusted if the integrands

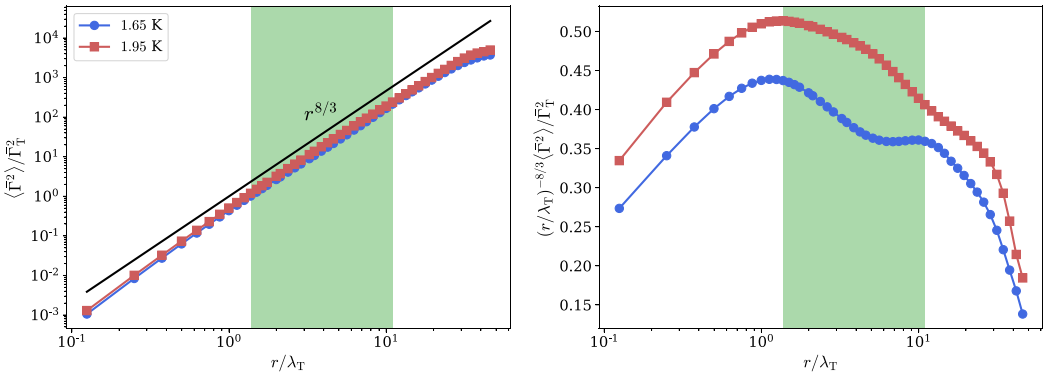

FIG. 2. Left panel: Circulation variance for the average of the experimental acquisitions at temperatures $T = 1.65$ K (blue circles) and $T = 1.95$ K (red squares). The green shaded area indicates the inertial range. The black solid line corresponds to Kolmogorov scaling law $r^{8/3}$. Right panel: Circulation variance compensated by Kolmogorov scaling.

$\Gamma^p P_r(\Gamma)$, for a given length scale within the inertial range, do not go to zero for the largest measured value of Γ, since the assumption $\langle\Gamma^p\rangle = \int_{-\infty}^{\infty}\Gamma^p P_r(\Gamma)d\Gamma \approx \int_{-\Gamma_c}^{\Gamma_c}\Gamma^p P_r(\Gamma)d\Gamma$, with Γ_c the circulation cut-off, breaks down. In Fig. 3, we also show the circulation integrands of the experimental measurements up to fourth order (in blue) for length scales within the inertial range. In

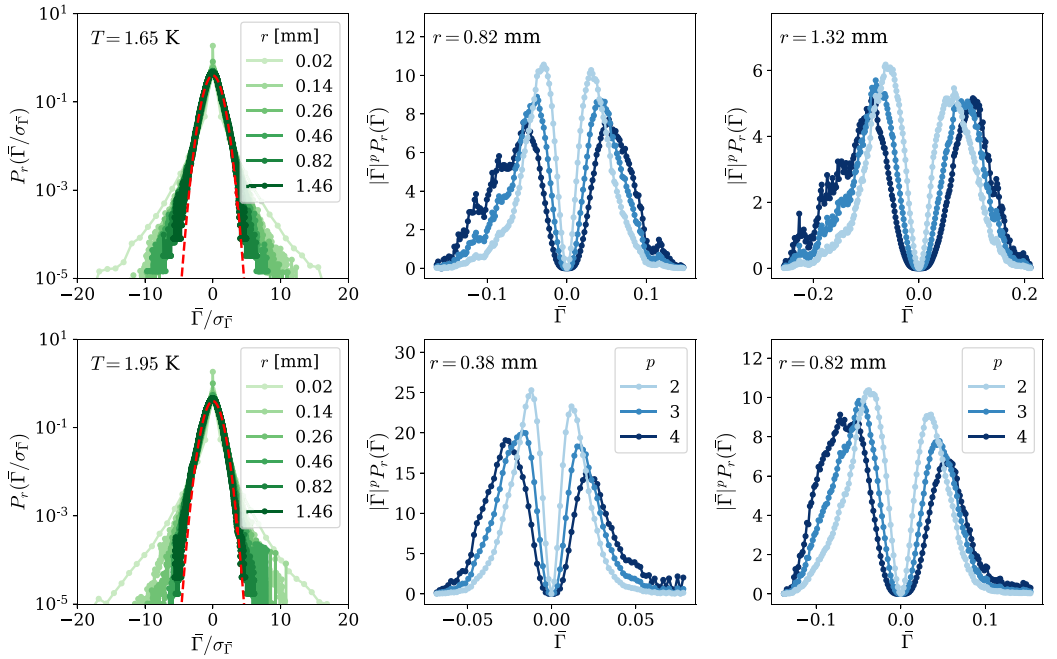

FIG. 3. Left panel: Experimental PDFs of the velocity circulation at different length scales. Each row corresponds to a different temperature. Middle and right panels: Circulation integrands up to moment four for two different length scales laying within the inertial range. The statistical convergence starts to fail on the fourth moment.

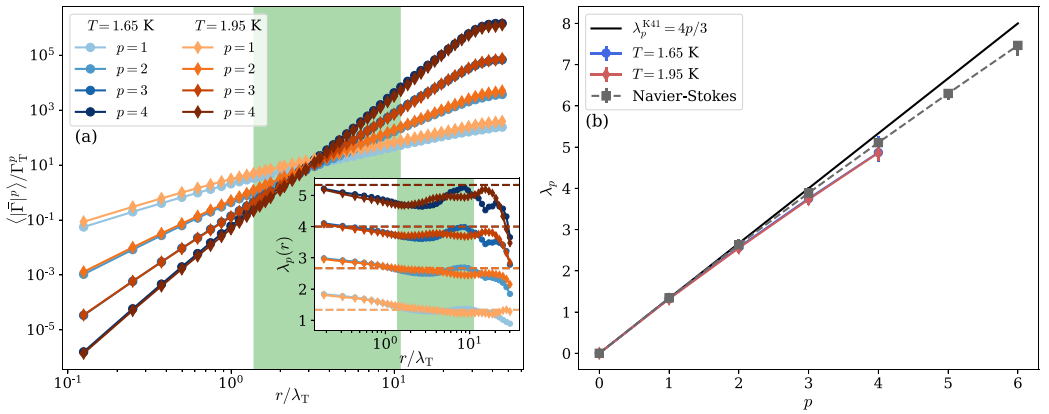

FIG. 4. (a) Circulation moments for the experimental data up to order four for temperatures $T = 1.65$ K (blue circles) and $T = 1.95$ K (orange diamonds). The inset shows the local slope of the circulation moments and Kolmogorov scaling as dashed horizontal lines. Green shaded areas indicate the inertial range for both temperatures. (b) Scaling exponents of the experimental measurements. The error bars indicate the maximum and minimum values of the local slope within the inertial range. As reference, we show Kolmogorov scaling $\lambda_p^{K41} = 4p/3$ and the scaling exponents of classical turbulence obtained from numerical simulations of the Navier–Stokes equations (gray squares).

particular, for the highest order shown here, the tails fail to converge for some scales. This behavior suggests that, at best, moment of order four are borderline in terms of statistical converge.

The circulation moments up to the fourth order for $T = 1.65$ K (blue circles) and for $T = 1.95$ K (orange diamonds) are shown in Fig. 4(a). Odd-order moments of circulation shall vanish as there is no preferential rotation of the flow inducing a symmetry breaking. Therefore, we study their absolute values $\langle|\Gamma|^p\rangle$. The local slopes, defined as the logarithmic derivative $\lambda_p(r) = d\log\langle|\Gamma|^p\rangle/d\log r$, approach to a plateau within the inertial range, obtaining the scaling exponents λ_p shown in Fig. 4(b). The error bars correspond to the maximum and minimum values of the local slopes in the inertial range. Up to the third order, the scaling exponents seem to follow the Kolmogorov scaling law for the circulation $\lambda^{K41} = 4p/3$. For higher orders, they start deviating from this prediction, taking smaller values and hence a stronger intermittency. As a reference, we show the scaling exponents of CT obtained from numerical simulations of the incompressible Navier–Stokes equations, taken from Ref. [28]. Our experimental data starts deviating from the classical limit for increasing order moments. However, data does not allow us to enforce this claim due to a possible lack of statistics to compute the fourth-order moment, as shown in Fig. 3. See Sec. IV for a further discussion.

B. HVBK results

The experimental results presented in Sec. III A provide evidence of circulation scaling in superfluid helium turbulence for low-order moments, in particular, observing a Kolmogorov scaling up to third order. However, the analysis of high-order moments cannot be completely trusted due to the lack of statistics. To provide insight on this aspect, we perform numerical simulations of the coarse-grained HVBK Eqs. (3)–(5) using typical parameters for superfluid ^{4}He (see Table I). We force the system with two independent random forces to obtain a stationary state of homogeneous isotropic QT (see Sec. II B for details on the model and numerical simulations). The two-fluid HVBK model describes the motion of the normal and the superfluid components at finite temperatures. Therefore, the turbulent properties of the flow may differ between them, so each velocity component, in principle, should be studied independently. Figure 5 shows the energy

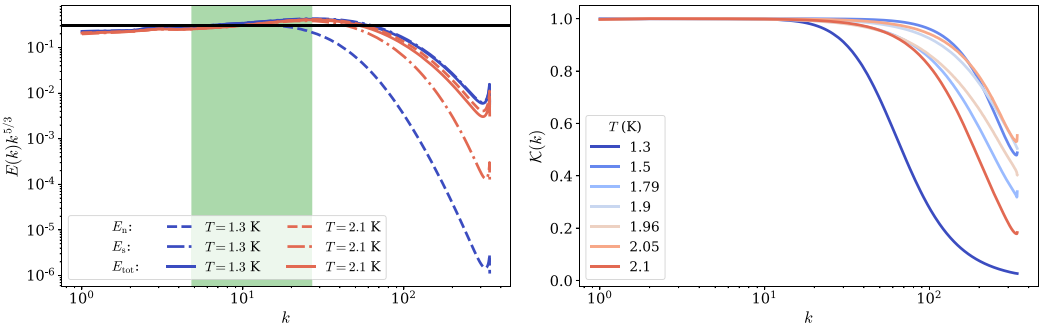

FIG. 5. Left panel: Spectra of the different energy components for the lowest and highest temperature of the simulations. Right panel: Velocity cross-correlation defined in Eq. (7) for different temperatures.

spectra of each velocity component in a statistically steady turbulent regime for two temperatures, the highest and lowest ones studied in this work. For both temperatures and velocity components, the energy spectra display a scaling close to Kolmogorov one $E_{n,s} \sim k^{-5/3}$ within an inertial range that varies depending on the temperature and the velocity component. The reason for these variations is that the normal and effective superfluid viscosities vary, and also present a different temperature dependence. One way of defining a homogeneous inertial range to facilitate the analysis of these two velocity components is by studying the total velocity field $\boldsymbol{v}_{tot} = \boldsymbol{j}/\rho$ with $\boldsymbol{j} = \rho_s \boldsymbol{v}_s + \rho_n \boldsymbol{v}_n$ the total momentum density.

The use of the total velocity could be valid under the assumption of *locking* between both velocity components, in the sense of $\boldsymbol{v}_n \approx \boldsymbol{v}_s$ [50,53]. One way of quantifying the scale-by-scale locking is with the velocity cross-correlation, [17,18]

$$\mathcal{K}(k) = \frac{2E_{ns}(k)}{E_n(k) + E_s(k)}, \tag{7}$$

with $E_{ns}(k)$ the cross-velocity energy spectrum associated to $\boldsymbol{v}_n \cdot \boldsymbol{v}_s$. If the cross correlation is equal to one, it indicates that both components are completely locked, while if it approaches to zero the superfluid and normal velocities are statistically independent. Figure 5(b) shows that for all temperatures the velocity components are locked with $\mathcal{K}(k) > 0.95$ at least up to $k \approx 50$ except for the lowest temperature case $T = 1.3$ K, where the locking stops at $k \approx 20$ as a consequence of the small proportion of normal density. In the inertial range, where the energy spectrum obeys Kolmogorov scaling, both fluid components are locked, so the study of the normal, superfluid, or total velocities should be statistically equivalent. Therefore, most of the following analysis on the velocity circulation is done using the total velocity.

The PDFs of the total velocity circulation normalized by its standard deviation $\sigma = \langle \Gamma^2 \rangle^{1/2}$ for different length scales are presented in Fig. 6. Here, length scales are normalized by the lambda microscale $\lambda_T = \sqrt{5E/\Omega}$ with $E = \int v^2/2dV$ the total energy of the system and $\Omega = \int |\boldsymbol{\omega}|^2/2dV$ the enstrophy. For all temperatures, the PDFs follow a qualitatively similar behavior as the one observed in the experiments discussed in Sec. III A (Fig. 3), with heavy tails for small scales and approaching a Gaussian for large scales. The circulation integrands show a good convergence up to order eight.

The circulation variance for different temperatures is shown in Fig. 7. The circulation is normalized by $\Gamma_T^2 = (\lambda_T^4/3)\langle |\boldsymbol{\omega}|^2 \rangle$, which corresponds to the small-scale prediction [27]. In this manner, when the normalized circulation variance is plotted as a function r/λ_T, the data collapses for all temperatures. For each individual temperature, the inertial range extends to a full decade. The green region corresponds to the intersection of all inertial ranges, corresponding also to scales where $\mathcal{K} > 0.95$. For all temperatures, the circulation variance follows a scaling close to the Kolmogorov one $\langle \Gamma^2 \rangle \sim r^{8/3}$. In the right panel, we show that the local slope approaches a plateau of $8/3$ within

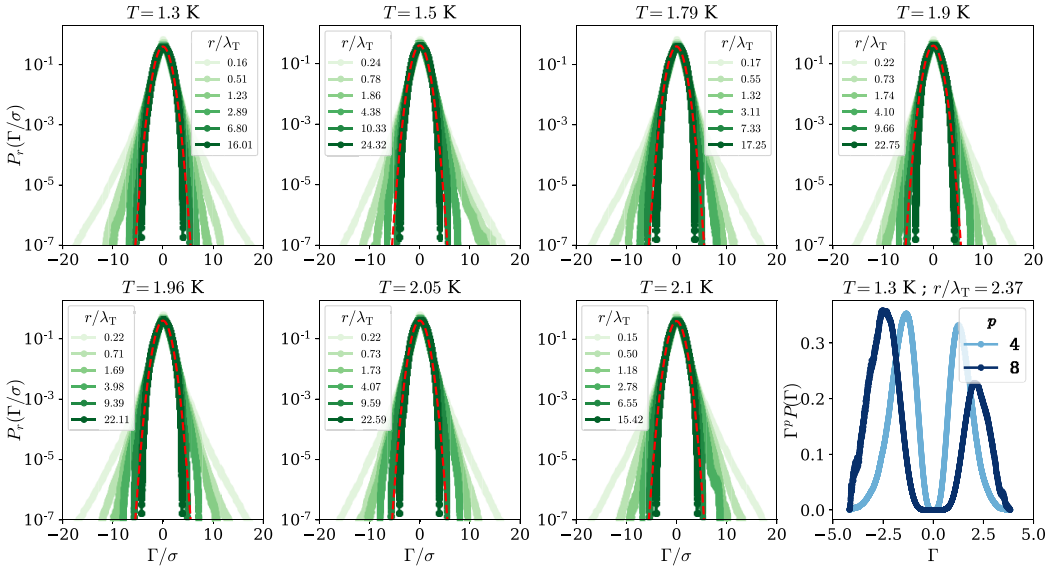

FIG. 6. Normalized PDFs of the velocity circulation Γ for different loop sizes at different temperatures. In red dashed lines, we show as reference a Normal distribution. The last panel shows the circulation integrands up to order eight for $T = 1.3$ K and a length scale within the inertial range.

the inertial range of scales. To analyze more in detail the temperature dependence of the system, we show the scaling exponents of the circulation variance as a function of the superfluid density ρ_s/ρ for the different velocity components in Fig. 8. The error bars correspond to the maximum and minimum values of the local slope in the inertial range. The different velocity components display no significant difference between themselves, supporting the argument of velocity locking. Also, in all cases there is no apparent temperature dependence and the exponents approach to Kolmogorov $\lambda_2^{\mathrm{K41}} = 8/3$. The temperature $T = 1.3$ K is removed from the normal velocity scaling due to the fact that the normal mass density is very small, displaying no clear scaling.

For high-order moments, the scaling exponents of the system seem to follow the same behavior observed in numerical simulations of the Navier–Stokes and GP equations [26,27], the latter represented by the shaded area in Fig. 9(a) which accounts for the error bars of data from Ref. [28]. For

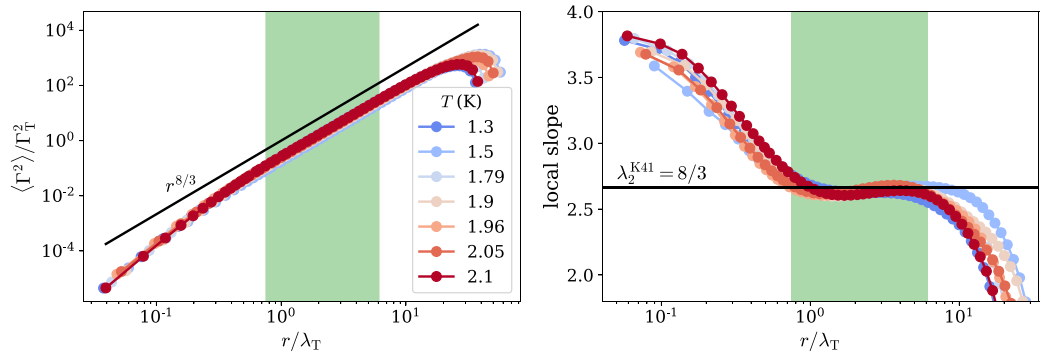

FIG. 7. Circulation variance of the total velocity $\boldsymbol{v}_{\mathrm{tot}}$ for different temperatures. Black solid lines correspond to Kolmogorov scaling. On the right, the local slope of the circulation variance, defined as the logarithmic derivative $d\log\langle\Gamma^2\rangle/d\log r$.

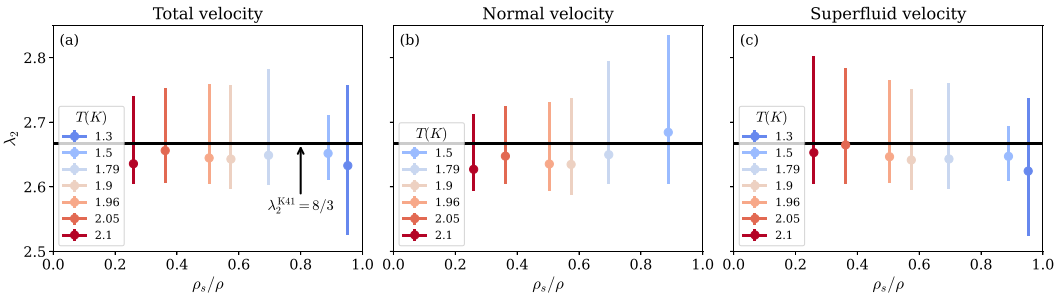

FIG. 8. Scaling exponents of the second-order moment of the velocity circulation at different temperatures for (a) the total velocity, (b) the normal velocity, and (c) the superfluid velocity fields. As a reference, the solid black line shows Kolmogorov scaling $\lambda_2^{K41} = 8/3$. Error bars indicate the maximum and minimum value of the local slope within the inertial range. The lowest temperature is removed from the middle panel due to the low mass density of the normal component.

$p \leqslant 3$, the scaling exponents of the velocity circulation follow Kolmogorov scaling $\lambda_p^{K41} = 4p/3$, while for higher-order moments up to $p = 8$ the scaling can be described by different multifractal models [26,28,29]. Figure 9(b) shows the scaling exponents from $p = 2$ to $p = 8$ as a function of the superfluid density. Horizontal dashed lines correspond to the exponents obtained in CT, and the gray area including its error bars. Here, it is clear that there is no apparent temperature dependence on the circulation scaling even for high-order moments, following in all cases the same behavior as in CT.

IV. DISCUSSION AND CONCLUSIONS

In this paper, we have addressed the scaling of circulation moments in superfluid helium at different temperatures. We have used superfluid grid turbulence experiments and numerical simulations of the HVBK model. We have compared the resulting circulation scaling exponents with those of Navier-Stokes (CT) and GP (zero-temperature QT) simulations from Ref. [28].

We obtained the scaling exponents for experiments at temperatures $T = 1.65$ K and $T = 1.95$ K up to order four. Remarkably, we have observed a clear Kolmogorov scaling for the circulation variance, and there is no apparent temperature dependence within the error bars. For the HVBK

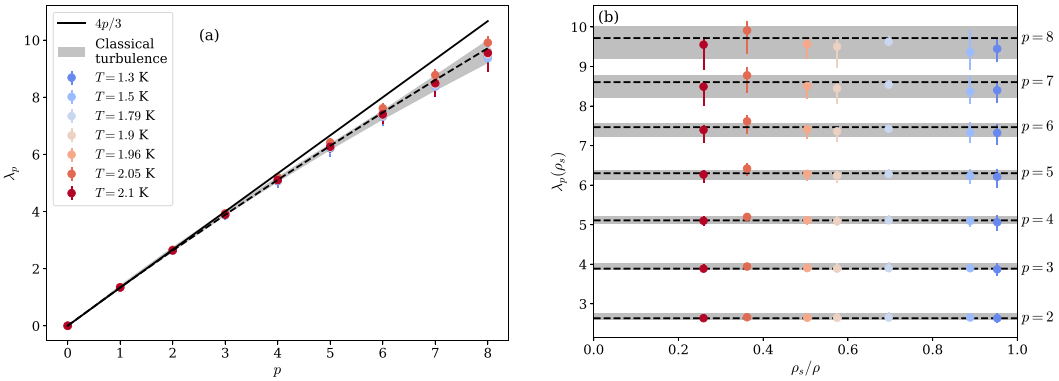

FIG. 9. Scaling exponent of the p-order moments of the velocity circulation at different temperatures. As a reference, the solid black line shows Kolmogorov scaling $\lambda_p^{K41} = 4p/3$ and gray shaded area shows the scaling obtained from numerical simulations of the Navier–Stokes equations, with the black dashed line its mean value.

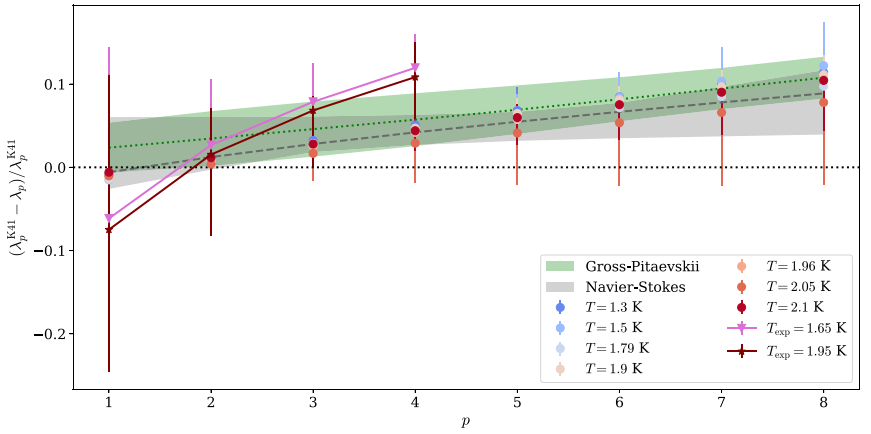

FIG. 10. Relative deviation of the circulation scaling exponents λ_p with respect to K41 prediction $\lambda_p^{K41} = 4p/3$. Data corresponds to superfluid grid turbulence experiments and numerical simulations of the HVBK, Gross-Pitaevskii, and Navier-Stokes models. Grid superfluid experiments are realized at two different temperatures ($T_{exp} = 1.65$K and $T_{exp} = 1.95$K). Exponents obtained from HVBK data of the current paper are at temperatures $T = 1.3$K-2.1K. Error bars are obtained by measuring the maximum and minimum of the local slope in the inertial range (see text). Classical and zero-temperature quantum turbulence exponents are taken from Navier-Stokes and Gross-Pitaevskii simulations of Ref. [28]. The green and gray areas show the error bars for those data sets, respectively.

numerical simulations, we have varied the temperature in the range $1.3 \leqslant T \leqslant 2.1$ K and observed that there is no clear temperature dependence either on the intermittent behavior both for low and high-order moments of velocity circulation. Furthermore, experimental and HVBK data coincide, within error bars, with classical and low-temperature QT simulations. This result is consistent with experimental observations of the velocity increments in superfluid helium [13,31]. Figure 10 presents the relative deviation $(\lambda_p^{K41} - \lambda_p)/\lambda_p^{K41}$ of the circulation exponents λ_p with respect to the Kolmogorov scaling λ_p^{K41} for all available data.

Note that if one drops error bars, there is a slight systematic departure of the experimentally measured circulation exponents from those obtained using HVBK simulations. First, one could be tempted to claim that such a deviation origins from the HVBK description of superfluid helium which might fail to capture the whole physics of superfluids. Indeed, the HVBK model provides only a coarse-grained description of superfluids and does not incorporate the dynamics of quantized vortices. Quantum vortices are related to singularities of the velocity field, which could impact high-order statistics. Whereas such singularities could affect velocity increments, they have no impact on circulation as it is perfectly well-defined for quantum vortices (it is actually quantized); see Ref. [27] for further discussion. Second, the available statistics used to compute high-order moments might not be enough to observe clean power laws in the inertial range, which could undoubtedly induce some errors. Finally, the circulation was computed using Eulerian fields constructed from Lagrangian particles. Several issues can arise from this method. For instance, a lack of particles in a given location of the flow could induce larger regions of constant velocity with abrupt jumps, affecting circulation values. Such regions are visible in the experimental Eulerian fields in Fig. 1(b). Moreover, particles might be trapped by superfluid vortices [34,36,37,43]. In that case, they cannot be considered perfect tracers, which will affect the determination of the Eulerian fields for which this assumption is crucial [54]. All those effects are difficult to quantify. On the other hand, the fact that the variance displays such a clear K41 scaling validates the current method and motivates its use for further studies. Whether the slight intermittency enhancement observed in experiments

has an actual physical origin or arises from the construction of the Eulerian fields is an interesting question that should be addressed in the future.

ACKNOWLEDGMENTS

We are grateful to J. I. Polanco for fruitful scientific discussions. This work was supported by the Agence Nationale de la Recherche through the GIANTE Project No. ANR-18-CE30-0020-01. This work was granted access to the HPC resources of CINES, IDRIS, and TGCC under the allocation 2019-A0072A11003 made by GENCI. Computations were also carried out at the Mésocentre SIGAMM hosted at the Observatoire de la Côte d'Azur. Y.T. and W.G. are supported by the National Science Foundation under Grant No. DMR-2100790 and the U.S. Department of Energy under Grant No. DE-SC0020113. They also acknowledge the support and resources provided by the National High Magnetic Field Laboratory at Florida State University, which is supported by the National Science Foundation Cooperative Agreement No. DMR-1644779 and the state of Florida.

[1] P. A. Davidson, *Turbulence in Rotating, Stratified and Electrically Conducting Fluids* (Cambridge University Press, Cambridge, 2013).
[2] A. N. Kolmogorov, Dissipation of energy in the locally isotropic turbulence, Proc. R. Soc. London A: Mathematical and Physical Sciences **434**, 15 (1991).
[3] U. Frisch, *Turbulence: The Legacy of A.N. Kolmogorov*, 1st ed. (Cambridge University Press, Cambridge, 1995).
[4] A. N. Kolmogorov, A refinement of previous hypotheses concerning the local structure of turbulence in a viscous incompressible fluid at high Reynolds number, J. Fluid Mech. **13**, 82 (1962).
[5] R. Benzi, G. Paladin, G. Parisis, and A. Vulpiani, On the multifractal nature of fully developed turbulence and chaotic systems, J. Phys. A: Math. Gen. **17**, 3521 (1984).
[6] Z.-S. She and E. Lévêque, Universal Scaling Laws in Fully Developed Turbulence, Phys. Rev. Lett. **72**, 336 (1994).
[7] C. F. Barenghi, L. Skrbek, and K. R. Sreenivasan, Introduction to quantum turbulence, Proc. Natl. Acad. Sci. **111**, 4647 (2014).
[8] L. P. Pitaevskii and S. Stringari, *Bose-Einstein Condensation and Superfluidity* (Oxford University Press, Oxford, 2016), Vol. 164.
[9] R. J. Donnelly, *Quantized Vortices in Helium II* (Cambridge University Press, Cambridge, 1991).
[10] J. Maurer and P. Tabeling, Local investigation of superfluid turbulence, Europhys. Lett. **43**, 29 (1998).
[11] L. Biferale, D. Khomenko, V. L'vov, A. Pomyalov, I. Procaccia, and G. Sahoo, Superfluid Helium in Three-Dimensional Counterflow Differs Strongly from Classical Flows: Anisotropy on Small Scales, Phys. Rev. Lett. **122**, 144501 (2019).
[12] J. I. Polanco and G. Krstulovic, Counterflow-Induced Inverse Energy Cascade in Three-Dimensional Superfluid Turbulence, Phys. Rev. Lett. **125**, 254504 (2020).
[13] E. Rusaouen, B. Chabaud, J. Salort, and P.-E. Roche, Intermittency of quantum turbulence with superfluid fractions from 0% to 96%, Phys. Fluids **29**, 105108 (2017).
[14] E. Varga, J. Gao, W. Guo, and L. Skrbek, Intermittency enhancement in quantum turbulence in superfluid He 4, Phys. Rev. Fluids **3**, 094601 (2018).
[15] Y. Tang, S. Bao, T. Kanai, and W. Guo, Statistical properties of homogeneous and isotropic turbulence in He II measured via particle tracking velocimetry, Phys. Rev. Fluids **5**, 084602 (2020).
[16] G. Krstulovic, Grid superfluid turbulence and intermittency at very low temperature, Phys. Rev. E **93**, 063104 (2016).
[17] L. Biferale, D. Khomenko, V. L'vov, A. Pomyalov, I. Procaccia, and G. Sahoo, Turbulent statistics and intermittency enhancement in coflowing superfluid ^{4}He, Phys. Rev. Fluids **3**, 024605 (2018).
[18] L. Boué, V. L'vov, A. Pomyalov, and I. Procaccia, Enhancement of Intermittency in Superfluid Turbulence, Phys. Rev. Lett. **110**, 014502 (2013).

[19] V. Shukla and R. Pandit, Multiscaling in superfluid turbulence: A shell-model study, Phys. Rev. E **94**, 043101 (2016).
[20] A. Migdal, Clebsch confinement and instantons in turbulence, Int. J. Mod. Phys. A **35**, 2030018 (2020).
[21] K. R. Sreenivasan, A. Juneja, and A. K. Suri, Scaling Properties of Circulation in Moderate-Reynolds-Number Turbulent Wakes, Phys. Rev. Lett. **75**, 433 (1995).
[22] N. Cao, S. Chen, and K. R. Sreenivasan, Properties of Velocity Circulation in Three-Dimensional Turbulence, Phys. Rev. Lett. **76**, 616 (1996).
[23] R. Benzi, L. Biferale, M. V. Struglia, and R. Tripiccione, Self-scaling properties of velocity circulation in shear flows, Phys. Rev. E **55**, 3739 (1997).
[24] K. P. Iyer, S. S. Bharadwaj, and K. R. Sreenivasan, The area rule for circulation in three-dimensional turbulence, Proc. Natl. Acad. Sci. **118**, e2114679118 (2021).
[25] Q. Zhou, C. Sun, and K.-Q. Xia, Experimental investigation of homogeneity, isotropy, and circulation of the velocity field in buoyancy-driven turbulence, J. Fluid Mech. **598**, 361 (2008).
[26] K. P. Iyer, K. R. Sreenivasan, and P. K. Yeung, Circulation in High Reynolds Number Iisotropic Turbulence is a Bifractal, Phys. Rev. X **9**, 041006 (2019).
[27] N. P. Müller, J. I. Polanco, and G. Krstulovic, Intermittency of Velocity Circulation in Quantum Turbulence, Phys. Rev. X **11**, 011053 (2021).
[28] J. I. Polanco, N. P. Müller, and G. Krstulovic, Vortex clustering, polarisation and circulation intermittency in classical and quantum turbulence, Nat. Commun. **12**, 7090 (2021).
[29] L. Moriconi, Multifractality breaking from bounded random measures, Phys. Rev. E **103**, 062137 (2021).
[30] G. B. Apolinário, L. Moriconi, R. M. Pereira, and V. J. Valadão, Vortex gas modeling of turbulent circulation statistics, Phys. Rev. E **102**, 041102(R) (2020).
[31] J. Salort, B. Chabaud, E. Lévêque, and P.-E. Roche, Investigation of intermittency in superfluid turbulence, J. Phys.: Conf. Ser. **318**, 042014 (2011).
[32] B. Mastracci and W. Guo, An apparatus for generation and quantitative measurement of homogeneous isotropic turbulence in He II, Rev. Sci. Instrum. **89**, 015107 (2018).
[33] B. Mastracci and W. Guo, Exploration of thermal counterflow in He II using particle tracking velocimetry, Phys. Rev. Fluids **3**, 063304 (2018).
[34] J. I. Polanco and G. Krstulovic, Inhomogeneous distribution of particles in coflow and counterflow quantum turbulence, Phys. Rev. Fluids **5**, 032601(R) (2020).
[35] B. Mastracci and W. Guo, Characterizing vortex tangle properties in steady-state He II counterflow using particle tracking velocimetry, Phys. Rev. Fluids **4**, 023301 (2019).
[36] Y. Tang, S. Bao, and W. Guo, Superdiffusion of quantized vortices uncovering scaling laws in quantum turbulence, Proc. Natl. Acad. Sci. **118**, e2021957118 (2021).
[37] U. Giuriato and G. Krstulovic, Interaction between active particles and quantum vortices leading to Kelvin wave generation, Sci. Rep. **9**, 4839 (2019).
[38] U. Giuriato and G. Krstulovic, Active and finite-size particles in decaying quantum turbulence at low temperature, Phys. Rev. Fluids **5**, 054608 (2020).
[39] Y. Tang, W. Guo, V. S. L'vov, and A. Pomyalov, Eulerian and Lagrangian second-order statistics of superfluid ^{4}He grid turbulence, Phys. Rev. B **103**, 144506 (2021).
[40] S. R. Stalp, L. Skrbek, and R. J. Donnelly, Decay of Grid Turbulence in a Finite Channel, Phys. Rev. Lett. **82**, 4831 (1999).
[41] L. Biferale, D. Khomenko, V. L'vov, A. Pomyalov, I. Procaccia, and G. Sahoo, Local and nonlocal energy spectra of superfluid 3He turbulence, Phys. Rev. B **95**, 184510 (2017).
[42] J. Koplik and H. Levine, Vortex Reconnection in Superfluid Helium, Phys. Rev. Lett. **71**, 1375 (1993).
[43] G. P. Bewley, M. S. Paoletti, K. R. Sreenivasan, and D. P. Lathrop, Characterization of reconnecting vortices in superfluid helium, Proc. Natl. Acad. Sci. U.S.A. **105**, 13707 (2008).
[44] A. Villois, D. Proment, and G. Krstulovic, Irreversible Dynamics of Vortex Reconnections in Quantum Fluids, Phys. Rev. Lett. **125**, 164501 (2020).
[45] G. Krstulovic, Kelvin-wave cascade and dissipation in low-temperature superfluid vortices, Phys. Rev. E **86**, 055301(R) (2012).

[46] E. Fonda, D. P. Meichle, N. T. Ouellette, S. Hormoz, and D. P. Lathrop, Direct observation of Kelvin waves excited by quantized vortex reconnection, Proc. Natl. Acad. Sci. **111**, 4707 (2014).
[47] C. Nore, M. Abid, and M. E. Brachet, Decaying Kolmogorov turbulence in a model of superflow, Phys. Fluids **9**, 2644 (1997).
[48] H. Homann, O. Kamps, R. Friedrich, and R. Grauer, Bridging from Eulerian to Lagrangian statistics in 3D hydro- and magnetohydrodynamic turbulent flows, New J. Phys. **11**, 073020 (2009).
[49] R. J. Donnelly and C. F. Barenghi, The observed properties of liquid helium at the saturated vapor pressure, J. Phys. Chem. Ref. Data **27**, 1217 (1998).
[50] L. Boué, V. S. L'vov, Y. Nagar, S. V. Nazarenko, A. Pomyalov, and I. Procaccia, Energy and vorticity spectra in turbulent superfluid ^{4}He from T = 0 to T_λ, Phys. Rev. B **91**, 144501 (2015).
[51] J. I. Polanco, N. P. Müller, and G. Krstulovic, Circulation.jl: Tools for computing velocity circulation statistics from periodic 3D Navier–Stokes and Gross–Pitaevskii fields, Zenodo (2021), https://doi.org/10.5281/ZENODO.5578953.
[52] F. Anselmet, Y. Gagne, E. J. Hopfinger, and R. A. Antonia, High-order velocity structure functions in turbulent shear flows, J. Fluid Mech. **140**, 63 (1984).
[53] W. F. Vinen and J. J. Niemela, Quantum turbulence, J. Low Temperature Physics **128**, 167 (2002).
[54] P. Švančara, D. Duda, P. Hrubcová, M. Rotter, L. Skrbek, M. L. Mantia, E. Durozoy, P. Diribarne, B. Rousset, M. Bourgoin, and M. Gibert, Ubiquity of particle–vortex interactions in turbulent counterflow of superfluid helium, J. Fluid Mech. **911**, 22 (2021).